

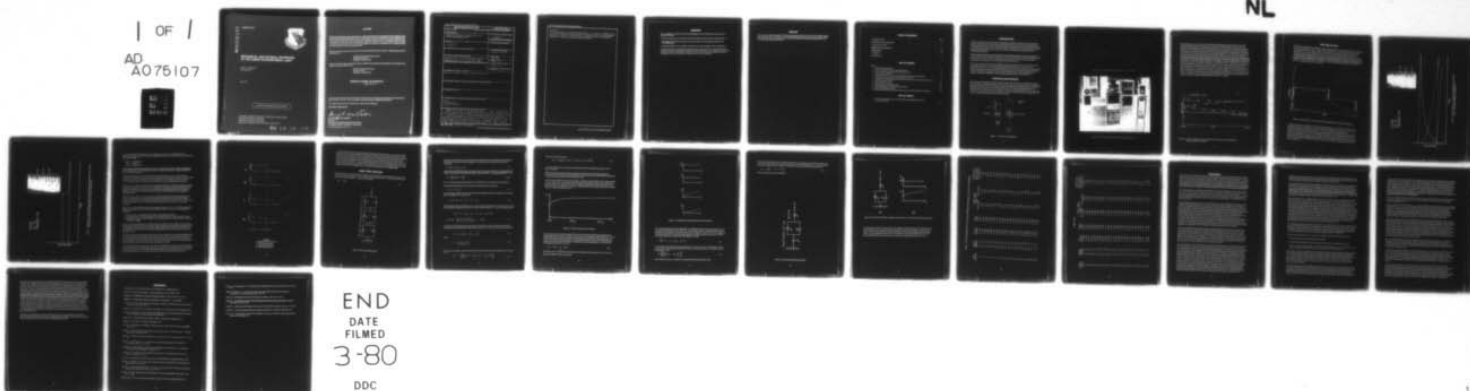
AD-A075 107

AEROSPACE MEDICAL RESEARCH LAB WRIGHT-PATTERSON AFB OH F/G 6/5
MECHANICAL AND PHYSICAL PROPERTIES OF THE HUMAN INTERVERTEBRAL --ETC(U)
JUN 79 L E KAZARIAN , I KALEPS
UNCLASSIFIED AMRL-TR-79-3

NL

1 OF 1

AD
A075107



END
DATE
FILMED
3-80
DDC

ADA075107

AMRL-TR-79-3



MECHANICAL AND PHYSICAL PROPERTIES OF THE HUMAN INTERVERTEBRAL JOINT

*LEON E. KAZARIAN
INTS KALEPS*

June 1979

Approved for public release; distribution unlimited.

**AIR FORCE AEROSPACE MEDICAL RESEARCH LABORATORY
AEROSPACE MEDICAL DIVISION
AIR FORCE SYSTEMS COMMAND
WRIGHT-PATTERSON AIR FORCE BASE, OHIO 45433**

79 10 16 118

NOTICES

When US Government drawings, specifications, or other data are used for any purpose other than a definitely related Government procurement operation, the Government thereby incurs no responsibility nor any obligation whatsoever, and the fact that the Government may have formulated, furnished, or in any way supplied the said drawings, specifications, or other data, is not to be regarded by implication or otherwise, as in any manner licensing the holder or any other person or corporation, or conveying any rights or permission to manufacture, use, or sell any patented invention that may in any way be related thereto.

Please do not request copies of this report from Aerospace Medical Research Laboratory. Additional copies may be purchased from:

National Technical Information Service
5285 Port Royal Road
Springfield, Virginia 22161

Federal Government agencies and their contractors registered with Defense Documentation Center should direct requests for copies of this report to:

Defense Documentation Center
Cameron Station
Alexandria, Virginia 22314

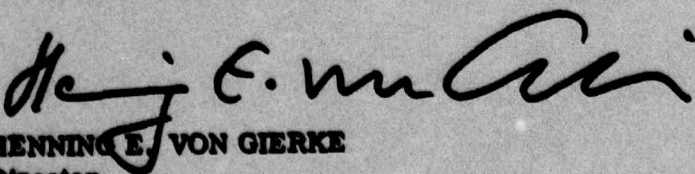
TECHNICAL REVIEW AND APPROVAL

AMRL-TR-79-3

This report has been reviewed by the Information Office (OI) and is releasable to the National Technical Information Service (NTIS). At NTIS, it will be available to the general public, including foreign nations.

This technical report has been reviewed and is approved for publication.

FOR THE COMMANDER



HENNING E. VON GIERKE
Director

Biodynamics and Bioengineering Division
Aerospace Medical Research Laboratory

SECURITY CLASSIFICATION OF THIS PAGE (When Data Entered)

REPORT DOCUMENTATION PAGE		READ INSTRUCTIONS BEFORE COMPLETING FORM
1. REPORT NUMBER AMRL-TR-79-3	2. GOVT ACCESSION NO.	3. RECIPIENT'S CATALOG NUMBER
4. TITLE (and Subtitle) MECHANICAL AND PHYSICAL PROPERTIES OF THE HUMAN INTERVERTEBRAL JOINT		5. TYPE OF REPORT & PERIOD COVERED Technical
7. AUTHOR(s) L. E. Kazarian I. Kaleps		6. PERFORMING ORG. REPORT NUMBER
9. PERFORMING ORGANIZATION NAME AND ADDRESS		8. CONTRACT OR GRANT NUMBER(s)
11. CONTROLLING OFFICE NAME AND ADDRESS Aerospace Medical Research Laboratory, Aerospace Medical Division, Air Force Systems Command, Wright-Patterson Air Force Base, Ohio 45433		10. PROGRAM ELEMENT, PROJECT, TASK AREA & WORK UNIT NUMBERS 62202F, 7231-14-04
14. MONITORING AGENCY NAME & ADDRESS (if different from Controlling Office)		12. REPORT DATE June 1979
		13. NUMBER OF PAGES 29
		15. SECURITY CLASS. (of this report) Unclassified
		15a. DECLASSIFICATION/DOWNGRADING SCHEDULE N/A
16. DISTRIBUTION STATEMENT (of this Report) Approved for public release; distribution unlimited		
17. DISTRIBUTION STATEMENT (of the abstract entered in Block 20, if different from Report)		
18. SUPPLEMENTARY NOTES		
19. KEY WORDS (Continue on reverse side if necessary and identify by block number) Joints Disk Degeneration Mechanical Properties		
20. ABSTRACT (Continue on reverse side if necessary and identify by block number) Human intervertebral joints were subjected to a constant stress and the resultant strain response was measured as a function of time. Thereafter, the stress was partially removed and the strain again measured as a function of time. Based upon the data, an analytical/mechanical model was formulated for which the Young's Moduli and a coefficient of viscosity were determined. The measured data indicate marked differences in the compressive behavior of the intervertebral joint excised from the thoracic and lumbar column. Several types of disk degeneration were observed and studied. It is suggested (CON'T)		

20 (Con't)

that the disk acts as a sealed pressurized unit. If tears or ruptures occur in the joint whereby nuclear fluid can easily escape from the intervertebral disk and be in direct contact with the vertebral centrum, the mechanical properties of the joint are significantly altered.

SUMMARY

This investigation has yielded several interesting findings on the intervertebral joint response to static compressive loading.

- When the normal intervertebral joint is subjected to loading, it clearly exhibits creep characteristics.
- The magnitude and character of the creep curve is a function of the morphologic condition of the intervertebral disk.
- If nuclear herniation occurs, the ability of the disk to carry axial compressive loads is compromised.

An analytical model corresponding to the experimental data was generated. The Young's Moduli and the coefficient of viscosity corresponding to the model were presented. There is some indication that the recovery mechanics of the intervertebral joint do not behave in a linear viscoelastic manner; additional analytical investigations are currently underway to determine the extent of this nonlinearity.

PREFACE

This work was initiated under project 7231-06-56 and completed under 7231-14-04, "Failure Characteristics of Spinal Elements." Mr. Ints Kaleps is with the Mathematical Analysis Branch; and the senior author is Chief, Biodynamic Effects Branch. Both branches are part of the Biodynamics and Bioengineering Division, AF Aerospace Medical Research Laboratory.

TABLE OF CONTENTS

INTRODUCTION	Page 4
MATERIALS AND METHODS	4
ANALYSIS OF DATA	7
CREEP CURVE ANALYSIS	12
DISCUSSION	20
SUMMARY	1
REFERENCES	24

LIST OF FIGURES

<i>Figure</i>	
1 The Creep Test Apparatus	4
2 Electrical Schematic of the Instrumentation System	5
3 The Creep Test Apparatus and Instrumentation System	5
4 Typical Normal Creep Plot	6
5 Salient Features of a Creep Curve Illustrating Elastic and Viscoelastic Regions	7
6 Typical Normal Creep Plot for a Normal Intervertebral Joint	8
7 The Effect of Vertebral Epiphysitis (Scheuermann's Disease) on the Deflection-Time Curve	9
8 Applied Compressive Stress	11
9 Three-Unit-Kelvin Chain	12
10 Typical Compressed Creep Response	14
11 Applied Stress at Individual Unit Strain Responses	15
12 Reduced Fluid Response Model	16
13 Reduced Solid Model and Respective Response Used for Final Coefficient Calculation	17

LIST OF TABLES

1 Test I.D., Spinal Segment, Area, Young's Moduli and Coefficient of Viscosity for Vertebral Units	18
---	----

INTRODUCTION

The intervertebral joint consists of the intervertebral disk, the adjoining vertebral centra with their paired posterior zygapophyseal articulations, and associated ligamentous structures. The intervertebral joint is a flexible structure that reacts as a hydraulic load absorber and transmitter. The joint reduces the jarring effects of mechanical vibrations and impact produced by walking, running, jumping, or any other activity, wherein the spinal column is subjected to movement or stress. The intervertebral joint is essential for normal mechanical spinal function.

This investigation evaluates biomechanical data collected while subjecting the human intervertebral joint to long-term axial compressive loading. The objectives of the experimental effort are to describe and measure the long-term creep response of the intervertebral joint in compression and to develop a theoretical model describing the creep mechanics for normal and diseased intervertebral joints.

The creep test measures the axial structural stability of the intervertebral joint. The test can be of relatively long duration; therefore it is of great biomechanical and clinical importance due to abnormal stress application, which may occur to surrounding hard and soft tissue structures. Creep tests are also important for analytic modeling of dynamic joint response and determining corresponding material property coefficients. Creep test information can be applied to many clinical and research areas, such as physical medicine, anatomy, orthopedics, rehabilitation, and for selecting suitable materials for disk replacement.

MATERIALS AND METHODS

The test apparatus illustrated in Figure 1 was used to measure creep and recovery. It consisted of an acrylic plastic container, a positioning box which had secured onto its base an acrylic plastic platen, a humidifier, lead weights, and associated electronic equipment. A linear voltage differential transformer (LVDT) was fixed to a side of the outer box, while its core was mechanically fixed to a side of the internal positioning box. An electrical schematic of the system is shown in Figure 2. Figure 3 is a photograph of the entire test system. The creep and recovery characteristics of 47 vertebral joints removed from four male cadavers, ranging in age from 27 to 46, were studied. Cause of death in each case was suicide.

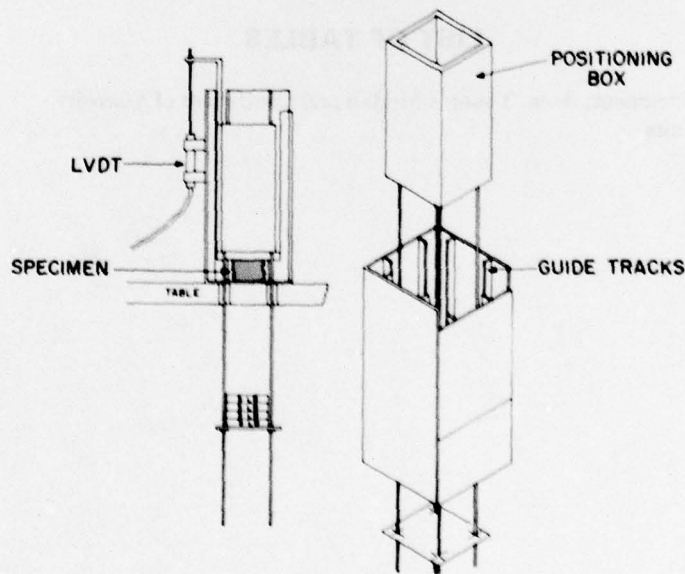


Figure 1. The Creep Test Apparatus

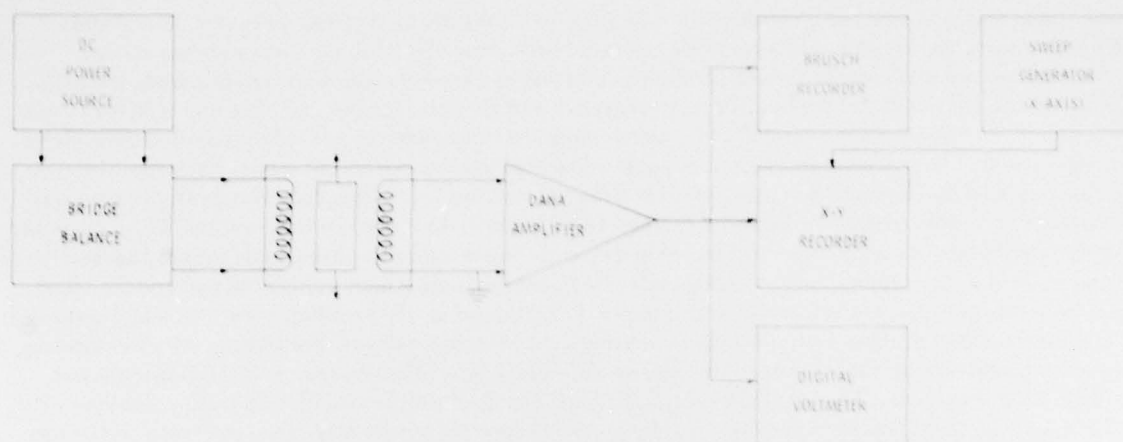


Figure 2. Electrical Schematic of the Instrumentation System



Figure 3. The Creep Test Apparatus and Instrumentation System

Each spinal unit was removed en masse within 24 hours following death. Anterior-posterior, lateral and oblique radiographs were taken. Using an electric band saw, parallel hard tissue slices were cut at each vertebral level perpendicular to the vertebral end plates and at a level of maximum vertebral body waisting. Each slice was cut parallel to the line of demarcation between the cartilaginous end plate and vertebral bone. This procedure was conducted carefully to avoid creating any nonuniformity of load distribution throughout the experiment. The posterior articular facet joints and spinal ligaments were left intact. Each specimen was labeled, inserted into a plastic bag, and placed in a deep freeze. Before testing, each vertebral specimen was removed from the deep freeze and allowed to stand 14-16 hours to thaw at room temperature. Throughout the thawing period, the specimen remained sealed in its plastic bag to minimize tissue dehydration. Just before the test procedure, each vertebral body-bearing surface was stamped onto a foam rubber ink pad and the inked specimen was stamped onto millimeter-scaled paper. From this print, the vertebral body area was determined. The initial height of the specimen was measured using a set of vernier calipers. For testing, the specimen was placed cephalad-side upwards between the platens of the creep box. (The posterior spinal column was not loaded, but free to tense.) The humidifier was turned on. The dead weight load of 30 lb (with a resulting total 40-lb weight applied to the specimen) was manually placed upon the weight tray. The total creep period was 8 hours \pm 1. Thereafter, the dead weight was removed, and the specimen allowed to recover for approximately 16 hours. During the recovery period the applied weight was 10 lb. Figure 4 illustrates a typical data plot. The direction of the arrows depicts the path taken by the pen of the X-Y recorder.

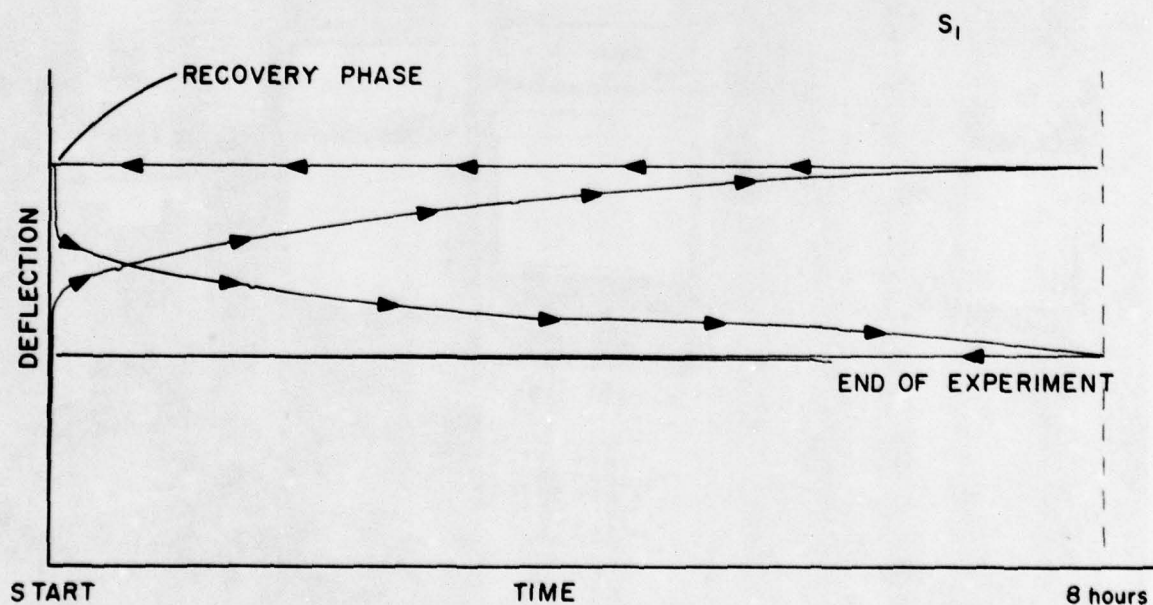


Figure 4. Typical Normal Creep Plot. The direction of the arrows depicts path taken by the pen of the X-Y recorder.

ANALYSIS OF DATA

When the intervertebral joint is subjected to a static compressive load, its structure will deform and adjust itself to oppose the applied force. Figure 5 illustrates the salient features of a typical normal creep curve for the intervertebral joint. The X-Y plotter displays an instantaneous compression immediately following load application. For very short loading times (less than 1 second), the deformation seems to consist of an instantaneous elastic deformation, Point A. The period after the initial deformation is followed by a period in which the predominant deformation is characteristic of a viscoelastic response, from Point A to Point B. In the next region, the curve approaches a low constant level. When the specimen is unloaded, an immediate increase in height is noted, Point B to Point C. Thereafter, the specimen gradually elongates but in no case does it recover to its original length, Point C to Point D.

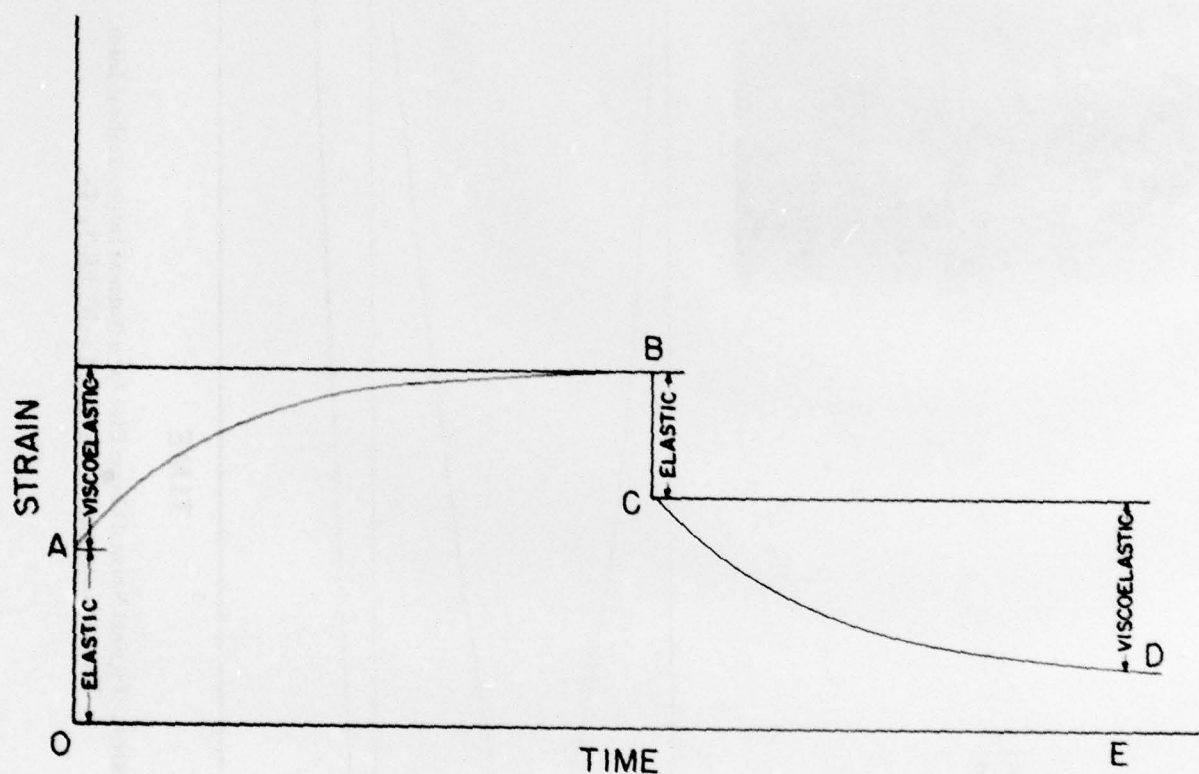


Figure 5. Salient Features of a Creep Curve Illustrating Elastic and Viscoelastic Regions

A typical creep curve for a normal intervertebral joint is illustrated in Figure 6. The pretest radiograph of the vertebral unit utilized to generate the curve is shown in the upper right hand corner of the curve. A curve for a diseased intervertebral joint is illustrated in Figure 7. Shown is the effect of vertebral epiphysitis (Scheuermann's Disease) on the creep response, along with a radiograph of the diseased joint. Figure 7 shows that the viscoelastic response of the intervertebral joint is obliterated. None of the data generated under this category was quantitated. Creep curves were also collected for various degrees of Schmorl's nodes, vertebral body fractures, divergent gradations of disk degeneration, and intervertebral disk protusion into the vertebral centrum. In each case the elastic portion of the curve was retained, while the viscoelastic portion of the creep curve was destroyed.

KCEB
T₆-T₇
5 MARCH 75

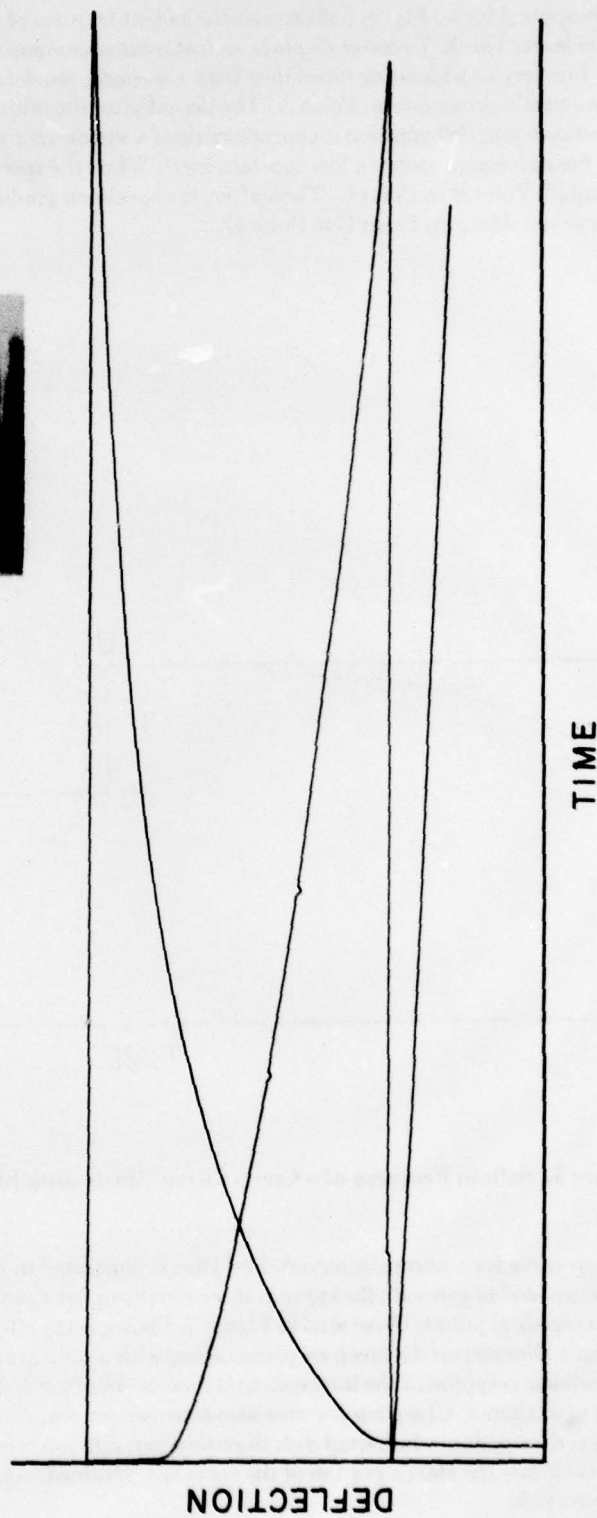
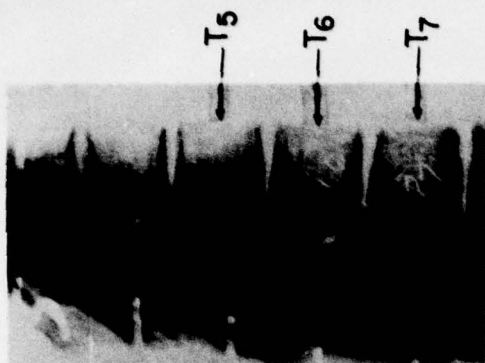


Figure 6. Typical Normal Creep Plot for a Normal Intervertebral Joint.
The test specimen is identified as KCEB-T₆-T₇.

KCEB
T₈-T₉
3 MARCH 75

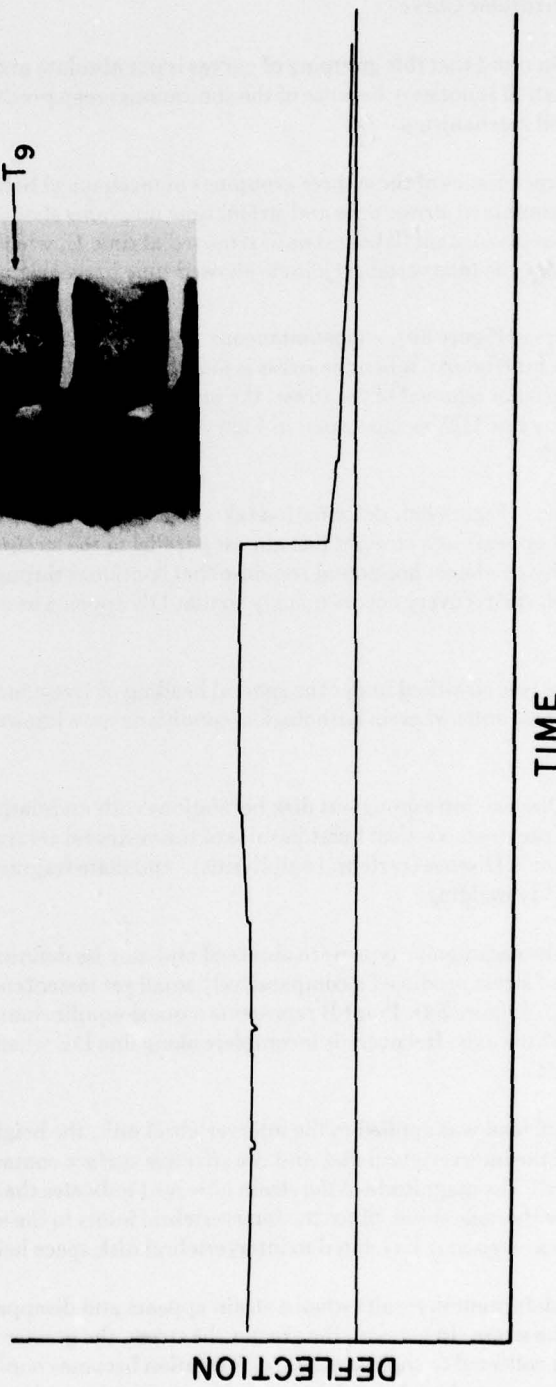
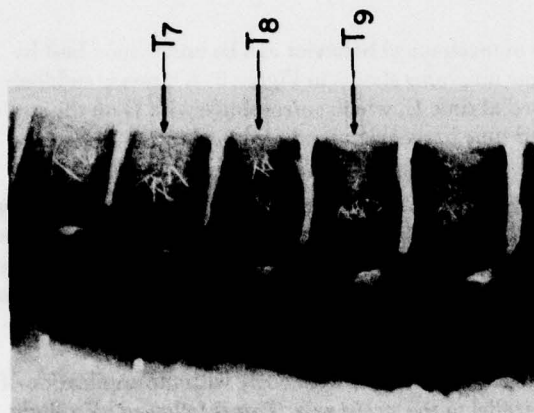


Figure 7. The Effect of Vertebral Epiphysitis (Scheuermann's Disease) on the Deflection-Time Curve.
Note obliteration of the viscoelastic phase as compared with Figure 6.

To conveniently identify particular creep curve characteristics, all curves were classified into three phenomenological types based on the respective amplitudes of the creep curve stages. These were identified as and called accordingly:

- Type 1 — Soft Solid Curve
- Type 2 — Solid Curve
- Type 3 — Irregular Curve

It must be kept in mind that this grouping of curves is not absolute and that certain overlap of characteristics exists. Interpretation is not easy because of the continuous creep processes and is not readily explained into discrete unrelated mechanisms.

The general characteristics of these three groupings of mechanical behavior can be understood best by considering the combined stress/time and strain/time diagrams shown in Figure 8. A stress is suddenly applied at time A and is kept constant (8 hours) until removed at time E, which corresponds with D on the strain curves. Thereafter, the intervertebral joint is allowed time to recover at reduced load (up to 24 hours).

In the Type 1 curve (Figure 8b), an instantaneous strain along AB is observed; this is followed by a progressive increasing strain for 8 hours. When the stress is maintained for a long time (>15 hours), the strain curve may equilibrate. On partial removal of the stress, the instantaneous component of the strain is always observed immediately along line DE, as illustrated in Figure 8. A recovery process follows; however, a permanent deformation is left.

In the Type 2 curve (Figure 8c), deformation takes place almost instantaneously with the application of the stress so that AB appears as a straight line almost parallel to the strain axis. This is followed by a slight transition, then by an almost horizontal response that continues throughout the period of stress. On removal of the stress at D, elastic recovery occurs quickly so that DE appears as a vertical line; recovery is usually incomplete.

The Type 3 curve was classified under the general heading of Irregular Creep Curve. This grouping included all the intervertebral units wherein pathological conditions were known to exist and were radiographically identified as:

1. Schmorl's Nodes: intraspongious disk herniations with undulating end plates.
2. Cleavage Fractures: vertical burst injuries of the vertebral centrum, with loss of end plate continuity.
3. Scheuermann's Disease (vertebral epiphysitis): end plate fragmentation, steplike deformity and anterior vertebral body wedging.

Creep curves of the rectangular type were observed and may be defined as curves of effectively zero viscosity. The application of stress produced a comparatively small yet instantaneous deformation represented by AB on the strain diagram (Figure 8d). Point B represents a quasi-equilibrium state under stress. Line BCD tends to be parallel to the time axis. Recovery is incomplete along line DE when the stress is removed. A permanent deformation is left.

Whenever an axial load was applied to the intervertebral unit, the height of the unit gradually diminished. The size and shape of the intervertebral disk and the effective surface contact area of the posterior articular facet joints were altered. The magnitude of the strain observed indicates that the lumbar spine exhibits more creep potential than the thoracic spine. Since the intervertebral joints in the upper thoracic spine are much thinner, this study suggests creep may be related to intervertebral disk space height.

A strictly elastic deformation results when a strain appears and disappears simultaneously with the application and removal of the stress. In general, the greater the stress, the greater the elastic deformation. Some evidence has recently been collected to suggest elastic deformation becomes nonlinear at high levels of stress. This may be related to the amount of *in vivo* weight carried by the particular intervertebral joint being tested.

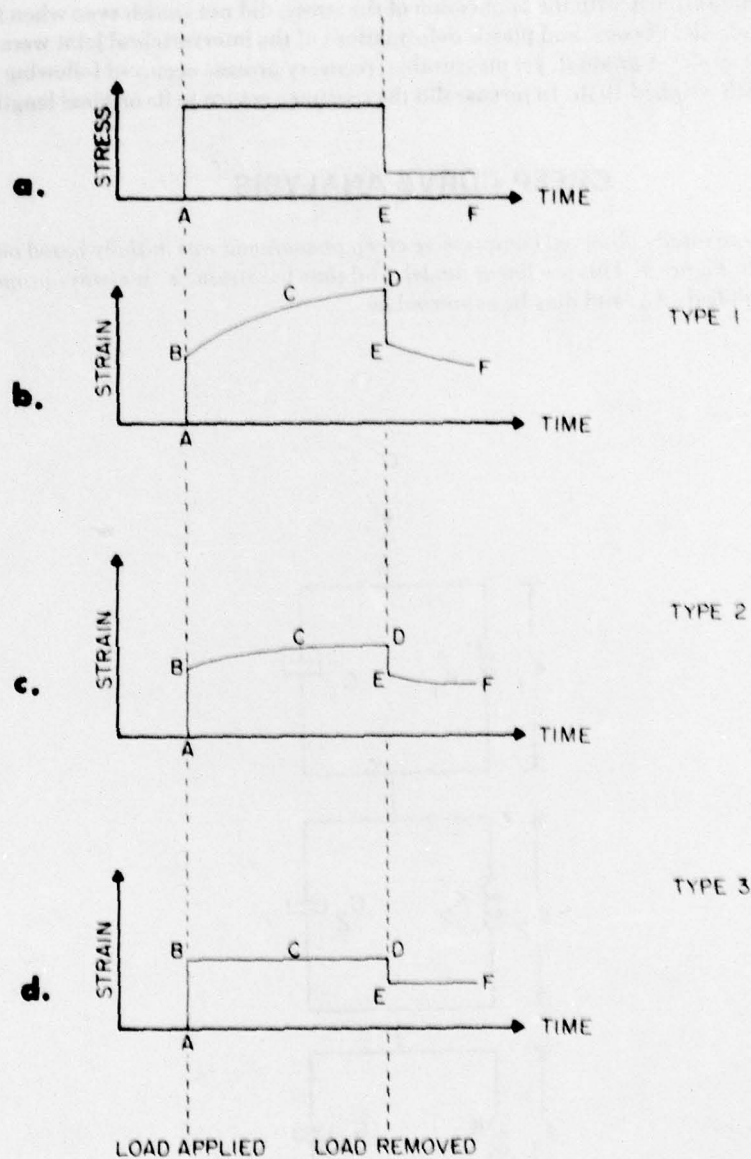


Figure 8
 a. Applied compressive stress
 b. Type 1 strain response
 c. Type 2 strain response
 d. Type 3 strain response

Viscoelastic deformation was observed following the initial elastic deformation phase. It was characterized by a high rate of creep that gradually diminished with time, but did not always attain a constant rate even after 8 hours of exposure to load. In addition to the elastic and viscous deformation properties observed, a third type of deformation may be defined: plastic deformation. This type of deformation occurred when the strain, which was observed simultaneously with the application of the stress, did not vanish even when the stress was removed. In this study, elastic, viscous, and plastic deformations of the intervertebral joint were recorded as a result of time-dependent strain. A gradual, yet measurable, recovery process occurred following removal of the applied load platen, which weighed 10 lb. In no case did the specimen return to its original length.

CREEP CURVE ANALYSIS

The analysis of the experimentally observed compressive creep phenomena was initially based on a three-unit-Kelvin model as shown in Figure 9. This is a linear model, and thus the strain, ϵ , is always proportional to the constant level of stress applied, σ_0 , and may be expressed as

$$\epsilon(t) = \sigma_0 J(t) \quad (1)$$

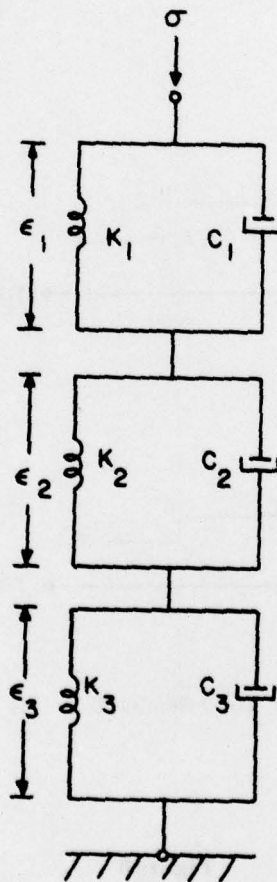


Figure 9. Three-unit-Kelvin Chain

The function $J(t)$ characterizes the particular material undergoing creep and is called the creep compliance. For the three-unit model, the total stress applied, σ , is equal to the stress across each unit and may be expressed by

$$\sigma = E_i \epsilon_i + \eta_i \dot{\epsilon}_i, \quad i = 1, 2, 3. \quad (2)$$

where the dot denotes differentiation with respect to time, E_i is Young's modulus, and η_i is the coefficient of viscosity for the respective units. These are related to the unit elasticity, k_i , and damping coefficient, c_i , by

$$E_i = \frac{k_i \Delta l}{A} \quad \text{and} \quad \eta_i = \frac{c_i \Delta l}{A} \quad (3, 4)$$

where Δl is the initial length of the specimen and A is the effective cross-sectional area of the specimen.

The individual strains of each of the three units were summed to give the total strain:

$$\epsilon = \epsilon_1 + \epsilon_2 + \epsilon_3 \quad (5)$$

By use of the three relations given by (2) and (5), the following differential equation relating stress and strain, as given by Flügge (1975), can be derived:

$$\sigma + p_1 \dot{\sigma} + p_2 \ddot{\sigma} = q_0 \epsilon + q_1 \dot{\epsilon} + q_2 \ddot{\epsilon} + q_3 \ddot{\epsilon} \quad (6)$$

By applying the Laplace transformation to (6), and assuming that all initial values of the time derivative terms are zero and that the applied stress at time $t=0$ is σ_0 , a constant, so that $\bar{\sigma}(s) = \sigma_0/s$, the following is derived:

$$\begin{aligned} \frac{\sigma_0}{s} (1 + p_1 s + p_2 s^2) &= (q_0 + q_1 s + q_2 s^2 + q_3 s^3) \bar{\epsilon}(s) \\ \text{or: } \bar{\epsilon}(s) &= \frac{\sigma_0 (1 + p_1 s + p_2 s^2)}{s(q_0 + q_1 s + q_2 s^2 + q_3 s^3)} = \sigma_0 \bar{J}(s) \end{aligned} \quad (7)$$

To solve for $\epsilon(t)$, first the roots for the polynomial in the denominator of $\bar{J}(s)$ must be determined and the expression split into partial fractions. If the roots are given by λ_1 , λ_2 and λ_3 , then $J(s)$ can be put in the form

$$\bar{J}(s) = \frac{1}{q_3} \frac{1}{s} \left(\frac{a_1}{s - \lambda_1} + \frac{a_2}{s - \lambda_2} + \frac{a_3}{s - \lambda_3} \right) \quad (8)$$

where

$$a_1 = \frac{1 + p_1 \lambda_1 + p_2 \lambda_1^2}{(\lambda_1 - \lambda_2)(\lambda_1 - \lambda_3)} \quad (9)$$

and a_2 and a_3 are similarly expressed by permutation of indices. Then an inverse transformation of (8) yields $\epsilon(t)$.

$$\epsilon(t) = - \frac{\sigma_0}{q_3} \left[\frac{a_1}{\lambda_1} (1 - e^{\lambda_1 t}) + \frac{a_2}{\lambda_2} (1 - e^{\lambda_2 t}) + \frac{a_3}{\lambda_3} (1 - e^{\lambda_3 t}) \right] \quad (10)$$

This can be rewritten in the form

$$\epsilon(t) = -\sigma_0 \left[A_1 (1 - e^{-\alpha_1 t}) + A_2 (1 - e^{-\alpha_2 t}) + A_3 (1 - e^{-\alpha_3 t}) \right] \quad (11)$$

A complete specification of $\epsilon(t)$ requires the determination of the six independent parameters A_i and α_i ($i = 1, 2$ and 3).

While an elaborate minimization scheme using experimental data may allow this determination, the characteristics of the experimental data indicated the use of an approximation method which led to calculated $\epsilon(t)$ values within approximately 5% of the measured values.

A typical experimental creep curve is shown in Figure 10. The time scale is divided into three regions indicated by ΔT_1 , ΔT_2 and ΔT_3 . It is assumed that within each region the predominant time response coefficient is α_1 , α_2 and α_3 , respectively; and further, that there is a minimal overlap of time-varying responses between the regions. That these assumptions were reasonable was demonstrated by the closeness of the fit of the calculated $\epsilon(t)$ curves with the measured data curves.

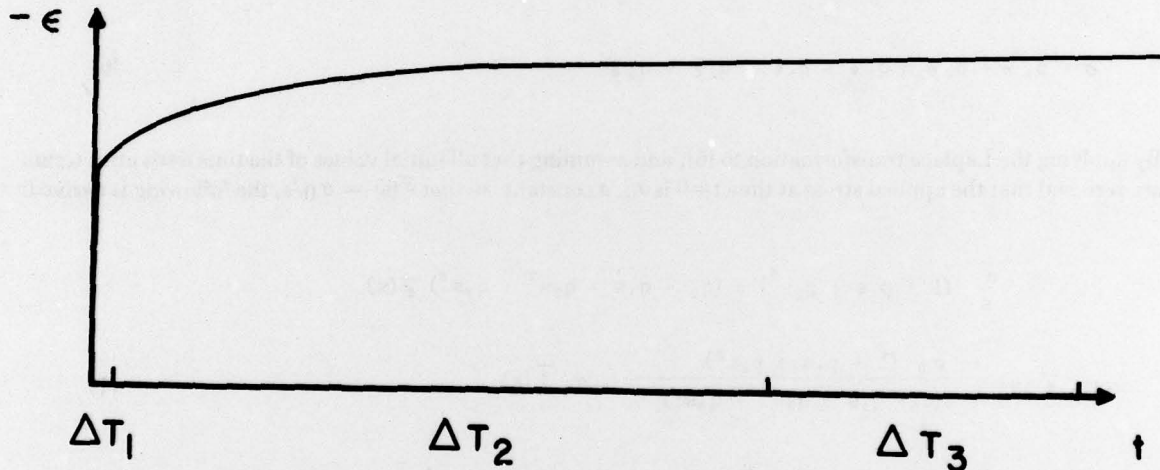


Figure 10. Typical compressed creep response

The analysis scheme was based on the observation that the creep response could be approximated by three superimposed responses, as shown in Figure 11. The ϵ_3 response corresponds to a Kelvin unit with $k_3 \rightarrow 0$ and exhibits a fluid response with a constantly decreasing length at a rate proportional to the applied stress. To examine the rate of pure fluid compression, it was assumed that the first two terms in Eq. (11) had attained maximal values at the termination of region ΔT_2 and that $\alpha_3 t$ was small within region ΔT_3 . This led to the following approximation for $\epsilon(t)$ in ΔT_3 .

$$\epsilon(t) = -\sigma_0 (A_1 + A_2 + A_3 \alpha_3 t) \quad (12)$$

By taking the derivative $\frac{d\epsilon(t)}{dt}$ and comparing it to the experimentally observed slope of $\epsilon(t)$ vs t in the ΔT_3 region, the coefficient $A_3 \alpha_3$ was determined.

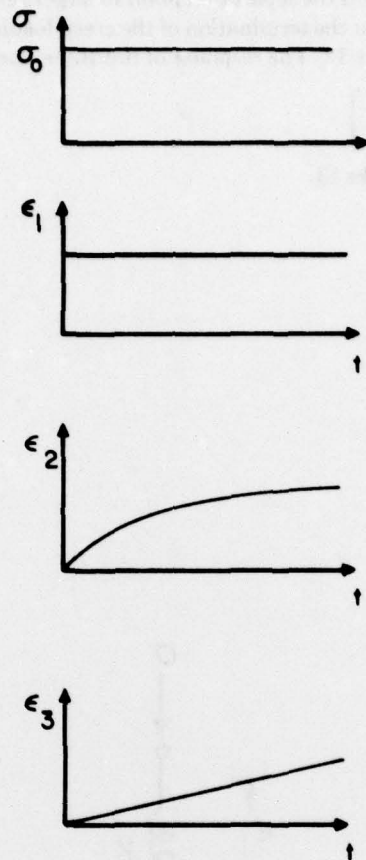


Figure 11. Applied Stress at Individual Unit Strain Responses

The exponential response observed in region ΔT_2 was modeled by a Kelvin unit with strain response ϵ_2 ; and the response in region ΔT_1 by a Kelvin unit with $c_1 \rightarrow 0$ and a strain response ϵ_1 that exhibits purely elastic properties. This approach led to a model structure as shown in Figure 10. Values for $A_1 + A_2$ were obtained by evaluating the equation at the maximum creep loading times measured (usually at about 8 hours). With the above approximations, an equation of the following form was written

$$\left(\frac{\epsilon(t)}{\sigma_0} + A_1 + A_2 - \alpha_2 A_2 t \right) = A_2 e^{\alpha_2 t} \quad (13)$$

A least-squares fit was made to this exponential function to solve for A_2 and α_2 . An optimization procedure was then applied which sought the minimum value for δ , by varying the location of the ΔT_2 and ΔT_3 region separation point, where

$$\delta = \left[\sum_{i=1}^N \left(\epsilon_{i(cal)} - \epsilon_{i(exp)} \right)^2 \right]^{1/2} \quad (14)$$

and $\epsilon_{i(cal)}$ and $\epsilon_{i(exp)}$ are, respectively, the calculated and experimental strain values.

The optimization technique tended to shift the separation point to larger time values and, in most of the cases analyzed, led to the result that $\epsilon_2 \gg \epsilon_3$ at the termination of the creep loading phase. For this reason the model was further simplified as shown in Figure 12. The response of this three-parameter model has the form

$$\epsilon(t) = -\sigma_0 \left[A_1 + A_2 (1 - e^{\alpha_2 t}) \right] \quad (15)$$

with a typical response as shown in Figure 13.

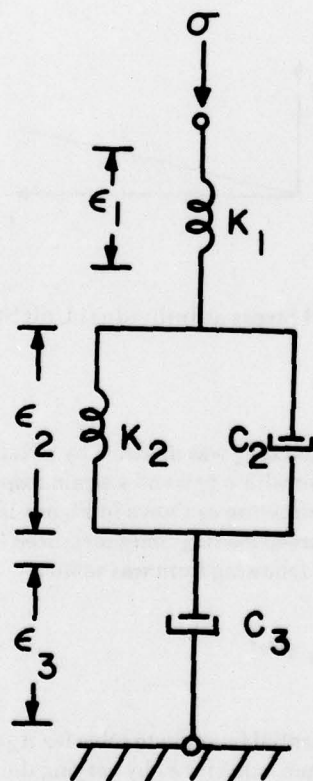


Figure 12. Reduced Fluid Response Model

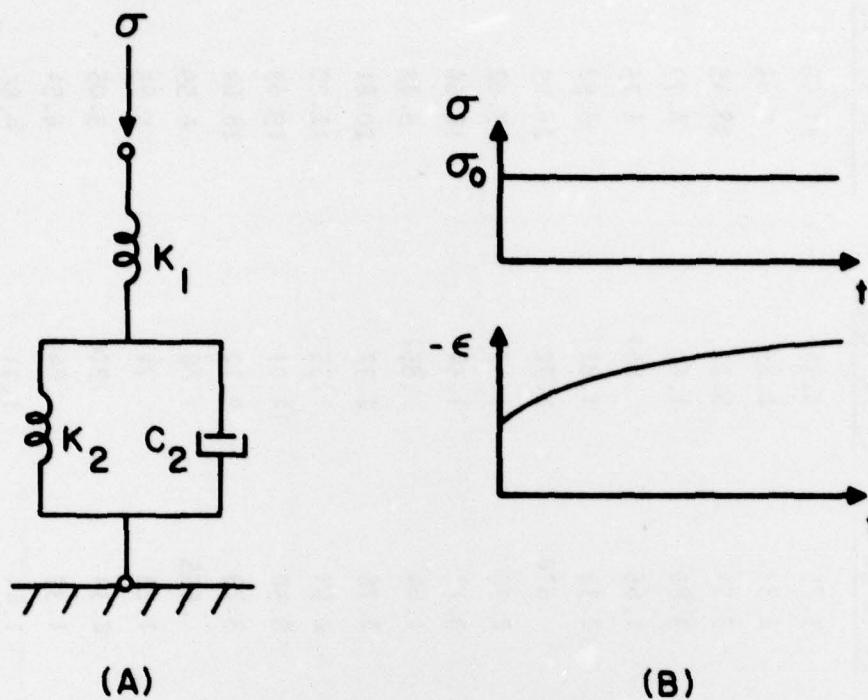


Figure 13. Reduced Solid Model and Respective Response Used For Final Coefficient Calculation

Using the above-described procedure, the data were analyzed on a digital computer (CDC 6600), and values were obtained for the Young's moduli and the coefficient of viscosity corresponding to the model shown in Figure 12. These values, together with specimen identification, initial area and height, are given in Table 1. Values of $\delta/\epsilon_{i(cal)}$ ranged from about 1% to 15% with about a 5% average using Equation (15) for the three-parameter model. Inclusion of a fluid term resulted in an insignificantly better fit of the data.

Table 1. Test I.D., Spinal Segment, Area, Young's Moduli and Coefficient of Viscosity for Vertebral Units

Test I.D. No.	Spinal Segment	Area (sq cm)	Height (cm)	Young's Moduli (Dynes/cm ²)		Coefficient of Viscosity (Dyne-sec/cm ²) η ($\times 10^{11}$)
				E_1 ($\times 10^8$)	E_2 ($\times 10^8$)	
1	T1 - T2	4.148	2.445	3.75	1.34	11.55
2	T2 - T3	5.619	2.515	2.33	2.89	5.83
4	T4 - T5	5.181	2.280	3.54	5.27	38.45
5	T5 - T6	5.568	2.085	3.80	1.60	8.77
6	T6 - T7	6.490	2.670	1.65	.867	6.25
7	T7 - T8	7.632	2.755	2.39	1.81	8.58
8	T8 - T9	8.123	1.194	.670	2.72	28.09
9	T9 - T10	7.781	2.240	2.90	1.43	17.02
10	T10 - T11	8.961	3.920	3.12	1.54	18.66
16	T2 - T3	5.787	2.431	1.44	.852	5.29
17	T3 - T4	5.148	2.585	6.76	2.32	20.81
18	T4 - T5	5.310	2.445	2.59	1.35	12.20
19	T5 - T6	5.800	2.240	6.50	14.01	19.63
20	T6 - T7	6.123	2.340	3.29	4.12	28.64
21	T7 - T8	8.161	2.670	.655	1.08	6.59
22	T8 - T9	8.032	2.615	1.26	.741	5.85
23	T9 - T10	9.123	2.670	2.34	.926	9.05
24	T10 - T11	10.329	2.795	1.39	.840	6.54
25	T11 - T12	11.800	3.515	1.44	1.21	9.86
26	T12 - L1	11.181	3.725	1.57	1.59	12.42
27	L1 - L2	11.813	3.900	.777	.729	5.39
28	L2 - L3	14.219	3.535	.827	.539	4.41

Table 1 (cont.)

Test I.D. No.	Spinal Segment	Area (sq cm)	Height (cm)	Young's Moduli (Dynes/cm ²)		Coefficient of Viscosity (Dyne-sec/cm ²) η ($\times 10^{11}$)
				E_1 ($\times 10^8$)	E_2 ($\times 10^8$)	
29	L3 - L4	14.168	3.165	2.010	0.829	8.71
30	L4 - L5	17.219	3.160	1.260	0.700	5.63
31	L5 - S1	25.613	3.760	0.794	0.699	4.93
42	L5 - S1	19.213	4.350	0.800	0.701	4.18
44	L3 - L4	19.639	4.090	2.080	4.810	11.27
45	L2 - L3	18.523	2.635	0.540	0.726	5.14
47	T11 - T12	19.348	2.789	1.280	0.599	3.83
48	T12 - L1	24.181	2.340	0.679	1.480	10.71
49	T9 - T10	19.987	2.171	0.770	0.415	2.16
50	T10 - T11	18.256	2.180	3.590	0.457	3.59
51	T8 - T9	17.110	2.163	0.712	0.694	4.33
52	T7 - T8	16.213	2.645	1.430	0.557	3.07
53	T4 - T5	14.032	1.965	1.410	2.550	2.60
54	T6 - T7	11.858	2.600	0.846	1.500	6.68
56	T5 - T6	14.729	1.980	0.532	1.990	11.46
57	T2 - T3	9.929	2.160	1.530	0.599	6.55
59	T9 - T10	16.813	2.775	0.369	0.527	11.20
60	T4 - T5	11.142	2.240	0.722	0.392	3.04
61	T5 - T6	10.432	1.895	1.140	0.491	4.62
62	T6 - T7	12.329	1.850	1.420	0.403	2.82
63	T11 - T12	16.503	2.975	1.030	0.656	11.51
64	T7 - T8	13.690	2.660	1.660	2.310	20.41
65	T10 - T11	14.561	2.765	1.640	0.633	10.65
66	T8 - T9	16.329	2.705	2.870	0.980	0.696
68	T12 - L1	16.503	2.935	1.600	0.575	10.62

DISCUSSION

The classical theory of elasticity deals with the mechanical properties of elastic solids, for which, according to Hooke's Law, stress is always directly proportional to strain in small deformations but independent of strain rate. The classical theory of hydrodynamics deals with the properties of viscous fluids, for which, according to Newton's Law, stress is always directly proportional to the rate of strain, but independent of the strain itself. The classical theories of elasticity and hydrodynamics are idealizations. Although the behavior of many solids approaches Hooke's laws for infinitesimal strains, and many liquids approach Newton's laws for infinitesimal rates of strain under other conditions, deviations are observed. Two types of deviations may be distinguished.

First, when finite strains are applied onto solids (those soft enough to substantially deform without breaking; e.g., annulus fibrosus), the stress-strain relations become much more complicated (non-Hookean). On the other hand, in steady-state flow with finite strain rates, many fluids (such as polymeric solutions; e.g., nucleus pulposus) exhibit marked deviations from Newton's Law (non-Newtonian flow). The dividing line between finite and infinitesimal is dependent on the level of precision under consideration. It varies greatly from one material to another.

Second, if both the strain and rate of strain are infinitesimal, a system may exhibit behavior which combines solidlike and liquidlike characteristics. For example, a substance or body which is not quite solid does not maintain a constant deformation under constant stress, but slowly deforms with time, or creeps. When such a body is constrained at constant deformation, the stress required to hold it gradually diminishes or relaxes. A body which is not quite liquid may, while flowing under constant stress, store some of the energy input instead of dissipating it; it may recover a portion of its deformation when the stress is removed (elastic recoil). Materials whose behavior exhibit such characteristics are identified as viscoelastic. If both strain and rate of strain are infinitesimal, the material may be viewed as possessing linear viscoelastic behavior. The intervertebral unit exhibits both elastic and viscous behavior through simultaneous dissipation and storage of mechanical energy. Material response to static loading can be explained by viscoelastic phenomena. The prominence of viscoelasticity in the intervertebral unit is not unexpected in light of the biomechanical studies of Virgin (1951, 1958), Hirsch and Nachemson (1954), Hirsch (1955), Yorra (1956), Evans and Lissner (1965), Yamada (1970), Kazarian (1972, 1975), Farfan (1973), Markolf and Morris (1974), and others.

The intervertebral disk forms the primary structural energy dissipation and transmission component of the intervertebral unit. The normal intervertebral disk is a fibrocartilaginous structure. It varies in size, shape, and thickness at different spinal levels. The disks in the cervical and lumbar regions are thickest to allow greater degree of motion. The disk is generally considered to be avascular; however, blood vessels within the disk have been reported by some investigators up to the age 25 (Beadle 1931), and nutritive canals have been observed to communicate directly with blood vessels of the spongiosa of the vertebral bodies (Bohmig 1930). The disk is made up of three integrated components: the nucleus pulposus and annulus fibrosus which are interposed between superior and inferior hyaline cartilaginous end plates.

The nucleus pulposus is the enclosed substance within the central part of the intervertebral disk surrounded by the annulus fibrosus. It consists of a three collagenous lattice enmeshed in a mucoprotein gel. The direction and arrangement of the nuclear network in the matrix frequently appear to be random, except at the upper and lower internal surfaces of the cartilaginous end plates where the nucleus pulposus is intimately and uniformly dispersed and attached to the end plates. The protein polysaccharide complex surrounding the interlacing collagenous fibrils endow the nucleus pulposus with an abundant water binding capacity (Rabinovitch 1961). Puschel (1930) reported that with advancing age, the water content of the disk progressively decreases. In the newborn the estimated water content is 88%, which gradually decreases to 65% at age 30, where it remains at a relatively constant level until old age. That is to say, to the third decade, the nucleus pulposus is a watery gelatinous substance. As growth rate subsides, a sequence of progressive events ensues that seems in effect to be a maturation process of the collagenous network. This process involves an increase in fibrillar structure and a change in their arrangement. The nuclear fibrils become thicker and, as a result, closely packed together, and also become unidirectionally oriented. Highly organized dense fibrillar arrays are fashioned from the original randomly distributed configuration. This process simultaneously involves a progressive dehydration of the mucoid material. Differences in biochemical composition appear, which are reported to be of a

degenerative nature and continue at an ever increasing rate, affecting both the intercellular matrix and cells. Cellular material derived from the surrounding annulus fibrosus and cartilaginous end plate gradually invade the nucleus pulposus; and the latter becomes fibrotic and desiccated (Sylvén 1951).

The annulus fibrosus emanates from the cartilaginous end plates and is composed of fibrous and cartilaginous elements in which the fibrous elements predominate. It is the first component of the intervertebral disk to reveal a complex collagenous architecture fully differentiated at birth (Armstrong 1958). The annulus fibrosus is present as a series of incomplete sheets or walls which surround the nucleus pulposus and constitutes the primary mass of the intervertebral disk. The annulus fibrosus develops in direct response to vertebral function and is capable of plastic adaptation to the exigencies of functional activity. It also varies in size, strength, and arrangement in the different regions of the spine (Armstrong 1958, Frost 1972).

The annular lamellae in the young adult form a dense, discrete, nearly concentric and obliquely asterisk-like interwoven structure. Each annular band runs an oblique parallel course. The directional obliquity of the fibers alternates in subsequent lamellae. The obliquity of the annular bands is greatest in the outermost regions of any given disk. The obliquity of the outermost annular walls also increases with ascending spinal levels. The interstratification angles of the annulus fibrosus tend to run helicoidally from one vertebral level to the next. The number of lamellae, their size, and obliquity of arrangement as well as their thickness show great variation for any given band within various parts of the same disk. The density of this fibrocartilaginous structure varies within the annular cross-sectional area. The lamellae tend to be closely packed anteriorly and posteriorly and less closely packed laterally (Galante 1967). The posterior lateral regions of the annulus fibrosus have marked irregularities and are less orderly. The lamellar bands do not form complete individual rings but intricately split or merge to interlock with other bands. The most peripheral fibers of the annular wall pass over the edges of the cartilaginous end plates and anchor themselves to and beyond the vertebral rim, to the margins of the adjacent vertebral centrum, and to its periosteum (Schmorl and Jungmanns 1971).

The cartilaginous end plates are intimately connected to the vertebral centra. In the early years of life, the end plates are structurally characterized as a homogenous, soft, pliable material with a translucent matrix, which is a complex protein (chondromucoid). Throughout the matrix is scattered an intricate array of intertwining "white fibers," which are reported to be "matted" and connected together, and macroscopically represent a "felt-work." Within this array are spaces containing cartilaginous elements (Cleland 1889).

Each end of the vertebral centrum is covered by one cartilaginous end plate. Its function is threefold.

- It protects the vertebral spongiosa from pressure atrophy;
- It confines the annulus fibrosus and nucleus pulposus within their anatomical boundaries; and
- It acts as a semipermeable membrane, which facilitates fluid exchange between the annulus fibrosus and nucleus pulposus and vertebral body via osmotic action (Crock 1973, Maroudas 1975).

In the early years of life, the end plates are loosely enmeshed with the irregular radiating fan-shaped ridges and furrows of the underlying vertebral centrum by a thin layer of calcified material (Schmorl and Junghanns 1971). Numerous minute vascular channels are embedded within and penetrate deeply into the cartilaginous plates from the vertebral side. These also permeate the annulus fibrosus. The end plate is adherent to the spicules of the underlying sieve-like surface of the vertebral centrum by a thin layer of calcified material. Between the fine, delicate spicules, the cartilaginous plate is in contact with the marrow through which it receives its nutrient substance.

With advancing age, the intervertebral disk undergoes a process of sequestration so that it ultimately becomes completely segregated from its confining structure. The nucleus pulposus becomes fragmented, stringy and dry in appearance. The mucoid structure of the nucleus is replaced by fibrocartilage. The annulus degenerates, losing its laminated-like appearance and structure. It becomes thin and unable to retain the sequestering nucleus (Lewin 1964). The vascular channels in the cartilaginous end plates diminish; by the third decade, the

vascular channels are largely obliterated. The remaining "holes" found in the cartilaginous plates are called "ossification gaps" and are ascribed as "scars" left by the obliteration of the vascular channels. Following the third decade, retrogressive changes occur in the hyaline cartilaginous end plates. The plates begin to show signs of ossification along with an increase in the deposition of calcium salts. The end plates gradually become brittle. Fibrillation becomes more evident and ranges from marked thinning to complete destruction of the central end plate zone (Schmorl and Junghanns 1971). When disintegration begins to occur, the deformation characteristics of this syndesmotic joint increase, its stability is compromised, and in consequence other structures in and about the involved joint must provide support and integrity. The fulcrum of levering forces is transferred toward the posterior articulating joints.

The intervertebral disk undergoes with aging a progressive architectural differentiation that is postulated to be a series of biochemical events in which there is a rapid breakdown of the protein polysaccharide linkages (DePalma and Rothman 1970).

In this experiment it is uncertain if there is any exchange of fluid taking place. Therefore, another mechanism of deformation may be concerned with the inherent material response of the intervertebral disk and specifically the geometry of the annulus fibrosus. Extensibility could occur in the annular walls by collagen fibril alignment (i.e., a change in orientation of the annular walls). Another deformation mechanism might be by rotation shearing or gliding and the stacking of neighboring annular walls with respect to their mutual boundaries. Still yet another mechanism might be the mass transport and redistribution of nuclear fluids radially by diffusion outward from the nucleus into vacancies within or between the annular walls.

Based upon a comparison between the combined Type 1 and 2 creep curves and the Type 3 creep curves, it is suggested that the disk forms a biomechanically-sealed pressurized unit following regression of the vasculature from the annulus fibrosus. The nutritional demands of the disk are fulfilled by the diffusion of lymph from the adjacent marrow cavities. This study also suggests that if the vertebral end plates lose their properties as a semipermeable membrane resulting from microtrauma or disease (Smith and Brown 1967), the water content of the nucleus pulposus decreases and a gradual architectural differentiation of the nucleus pulposus and annulus fibrosus probably takes place. Based upon these observations, it may also be surmised that the weight bearing and load transmission characteristics of the intervertebral joint are altered. Mechanical loads are spread over a larger surface contact area, and osteophytes form along the edges of the vertebral centrum and at the articular facet joints to transmit and attenuate loads.

How realistically the creep observed in the experiments reported herein is related to the *in vivo* situation is uncertain. *In vivo*, the intervertebral joint is subject to complex, nonuniform loading. Second, the load transmission pathways in the spinal column are dependent largely upon overall spinal column geometry and the physiologic condition of the intervertebral disks and articular facet joints. The intervertebral joint cannot be considered as a simple structure.

To shed further light on the mechanisms of intervertebral joint creep, it is convenient to consider three types of experiments as constituting the future work to be conducted in the field of intervertebral joint creep and recovery. The first is the determination of the effects on creep parameters of different conditions of stress, temperature, humidity, and anatomical and physiological variables. Based on such information, relationships between stress and intervertebral joint condition for a particular mechanical load or creep rate can be formulated. Thus, advantage can be taken of such relationships for interpolation or extrapolation purposes or both.

The second type of experiments is the determination of the methods by which the intervertebral joint undergoes deformation during creep. From such observations, particular modes, mechanics, and processes of deformation should be defined in detail. The individual physiologic mechanisms of disk action and their subsequent short- and long-term pathomechanical effects on hard and soft tissues will contribute new knowledge as to the etiology of degenerative changes in the vertebral centra and posterior articular facet joints. The invasion of nuclear tissue into the cancellous bone of a vertebral body instigates a biochemical reaction between the hematopoietic tissue of the centrum and the semifluidic nucleus pulposus, and gradually

transforms the herniated material into a cartilaginous nodule which in time is surrounded by sclerosed bone. With time, the cartilaginous nodule shows up on a roentgenogram encircled by an excavated shallow bony concavity. The size of the concavity varies from the head of a pin to that of a lentil bean. If hairline stellate fractures or tears are present in an end plate, open channels are created that lead to avenues of nuclear dehydration. The intervertebral joint space becomes narrowed due to intervertebral disk thinning. If, on the other hand, larger amounts of nuclear material are prolapsed, diminution of the intervertebral disk space is noted. In either case, depending upon the amount of nuclear tissue prolapsed, the stress created by constant weight bearing is transferred to the articular facet joints. Adjacent vertebrae may undergo sclerosis with the formation of bony lippling and spurring. The articular facet joints may show atrophy of the articular cartilage, eburnation and erosion of bony surfaces. Is a joint which shows those pathologic changes able to withstand excessive mechanical forces? This biomechanical study has shed additional information on the prolapse of nuclear tissue through the cartilaginous end plate into the vertebral centrum. The evidence collected herein strongly suggests that spinal mechanics are altered as a result of nuclear tissue prolapse. The connection between clinically observed pathology, secondary spinal deformities, microtrauma and fracture potential is currently open to further examination. Knowledge of the mechanical response of nuclear tissue prolapse will eventually establish certain prophylactic restrictions on certain activities, so that the danger of further spinal injury potential is reduced.

The third type of experiment is concerned with the kinetics of flow, the nonuniformity of stress (both in direction and magnitude), and the formulation of relationships connecting the external variables of stress and ligamentous prestress with the amount and rate of intradiskal fluid exchange.

REFERENCES

- Armstrong, J. R.: *Lumbar Disc Lesions*. E & S Livingston, Ltd., Edinburgh, 1958.
- Beadle, O.: *The Intervertebral Disks*. London, His Majesty's Stationary Office, 1931.
- Bohmig, R.: Die Blutgefassversorgung Der Wirbelbandscheiben. *Arch. f. Chir* 158: 374, 1930.
- Cleland, C.: On Fibro-Plates and Intervertebral Discs. *J. Anat. Physiol.*, 24: 373, 1889.
- Crock, H. et al: Observations on the Venous Drainage of the Human Vertebral Body. *Journal of Bone and Joint Survey*, Vol 55B: 528, 1973.
- Depalma, A., and Rothman, R.: *The Intervertebral Disc*. W. B. Saunders Company, Philadelphia, 1970.
- Evans, G., and Lissner, H.: Studies on the Energy Absorbing Capacity of Human Lumbar Intervertebral Discs. 7th Stapp Car Crash Conference Proceedings, 1965.
- Farfan, H. F.: *Mechanical Disorders of the Low Back*. Lea and Febiger, Philadelphia, 1973.
- Flügge, W.: *Viscoelasticity*. Springer-Verlag, Berlin, 1975.
- Frost, H.: *The Physiology of Cartilaginous, Fibrous and Bony Tissue*. Charles C. Thomas, Springfield, Illinois, 1972.
- Galante, G.: Tensile Properties of the Human Lumbar Annulus Fibrosus. *Acta Ortho Scand — Suppl 100*, Munksgaard, Copenhagen, 1967.
- Hirsch, C.: The Reaction of Intervertebral Discs to Compression Forces. *J. Bone & Joint Surg.*, 37-A: 1188, 1955.
- Hirsch, C., and Nachemson, A.: New Observations on the Mechanical Behavior of Lumbar Discs. *Acta Orthop. Scand.*, 23: 254, 1954.
- Kazarian, L.: Dynamic Response Characteristics of the Human Vertebral Column. *Acta Orthopaedica Scandinavica #146*, Munksgaard, Copenhagen, 1972.
- Kazarian, L.: Creep Characteristics of the Human Spinal Column. *The Orthopaedic Clinics of North America*, Vol 6 (No. 1): 3, 1975.
- Lewin, T.: *Osteoarthritis in Lumbar Synovial Joints*. Orstadius Boktryckeri Aktiebolag Goteborg, 1964.
- Markolf, K., and Morris, J.: The Structural Components of the Intervertebral Disc. *Journal of Bone and Joint Surgery*, 56A: 686, 1974.
- Maroudas, A., Stockwell, R., Nachemson, A., Urban, J.: Factors Involved in the Nutrition of the Human Lumbar Intervertebral Disc. *J. Anat.*, 120: 113, 1975.
- Puschel, J.: Der Wassergehalt Normaler Und Degenerierter Zwischenwirbelscheiben. *Beitr. Path. Anat.*, 84: 123, 1930.
- Rabinovitch, R.: *Diseases of the Intervertebral Disc*. Charles C. Thomas, Springfield, Illinois, 1961.

- Schmorl, G., and Junghanns, H.: *The Human Spine in Health and Disease*. Grune and Stratton, New York, 1971.
- Smith, L., and Brown, J.: Treatment of Lumbar Intervertebral Disk Lesions by Direct Injection of Chymopapain. *J. Bone and Joint Surg.*, 49B: 502, 1967.
- Sylvén, B.: On the Biology of the Nucleus Pulposus. *Acta Orthop. Scand.*, 20: 275, 1951.
- Virgin, W.: Experimental Investigation into the Physical Properties of the Intervertebral Disc. *J. Bone & Joint Surg.*, 33-B: 607, 1951.
- Virgin, W.: Anatomical and Pathological Aspects of the Intervertebral Disc. *Indian J. Surg.*, 20: 113, 1958.
- Yamada, H.: *Strength of Biological Materials*. Williams and Wilkins Co., Baltimore, Maryland, 1970.
- Yorra, A. J.: *The Investigation of the Structural Behavior of the Intervertebral Disc*. Thesis. Massachusetts Institute of Technology, 1956.